Circuit Modeling of Rotating Magnetic Field Field-reversed Configuration Thrusters

Joshua M. Woods*, Benjamin A. Jorns†, and Alec D. Gallimore‡
University of Michigan, Ann Arbor, MI, 48109

A lumped circuit model is presented for the formation and propagation of a rotating magnetic field field-reversed configuration thruster. The driving coils are treated as two lumped circuit inductors operated 90° out of phase. The plasma is modeled as an inductive load with capacitive and resistive elements, and a series of equations are derived based on Kirchhoff's laws and charge continuity. Plasmoid translation is captured by modeling the whole plasma as a conducting slug undergoing acceleration due to the Lorentz force. Two operating regimes are analyzed: the system with coupling to the plasma and the case in which the ring down of the coils during discharge is fixed. It is found that for high input energies, the efficiency scales inversely with input energy. In addition, several notable trends can be observed in the numerical data. Both specific impulse and efficiency increase with coupling. There is also indication of an optimum efficiency as input energy changes. These observed trends are discussed in the context of projected thruster performance.

I. Nomenclature

α	=	damping factor
B_o	=	amplitude of the RMF
$\vec{B_{RMF}}$	=	rotating magnetic field due to RMF coils (r and θ subscripts denote directions in cylindrical coordinates)
$\vec{B_s}$	=	steady background magnetic field (r and z subscripts denote directions in cylindrical coordinates)
C	=	circuit capacitance
e	=	elementary charge
E_o	=	input energy
I	=	impulse
I_{sp}	=	specific impulse
$I_{x,y}$	=	coil currents
$\vec{J}$	=	plasma current densities (θ and z subscripts denote directions in cylindrical coordinates)
k	=	coupling factor
L	=	self-inductance of the RMF coils
l_p	=	length of the plasma slug
l_s	=	length of RMF coils
N	=	number of turns in RMF coils
n	=	plasma density
η	=	plasma resistivity
η_E	=	thruster efficiency
$\phi_{x,y}$	=	magnetic flux
R	=	driver coil circuit resistance
RMF	=	rotating magnetic field
r_p	=	radius of the plasma slug
u_{ex}	=	exit velocity of the plasma slug
V_o	=	initial capacitor voltage
ν_{ei}	=	electron-ion collision frequency
ω	=	RMF frequency

*AIAA Student Member, Aerospace Engineering, 1320 Beal Ave, Ann Arbor, MI 48109
†AIAA Senior Member, Aerospace Engineering, 1320 Beal Ave, Ann Arbor, MI 48109
‡AIAA Senior Member, Aerospace Engineering, 1320 Beal Ave, Ann Arbor, MI 48109

II. Introduction

Traditional chemical rockets have long propelled our spacecraft to destinations across the solar system. However, their low specific impulses (I_{sp}) translates directly into poor fuel economies. A more efficient propulsion system is necessary if we are to ever embark on manned space exploration or other missions requiring high payload masses past cislunar space at a reasonable launch cost. Electric propulsion (EP) devices have been researched for decades to fill this niche. As opposed to chemical rockets which harness the thermal energy released by propellant molecules during combustion, EP utilizes external power sources to convert electrical energy to kinetic energy. In doing so, propellant molecules are able to be accelerated to exhaust velocities much higher than those found in chemical propulsion systems resulting in higher overall I_{sp}'s [1]. There are several types of EP systems with two of the most well known and utilized state of the art systems being Hall and ion thrusters. These devices' specific impulses' range from 10^3 - 10^4 s and can reach efficiencies above 60% [2]. Nevertheless, when one looks at landscape of EP devices available, it becomes apparent that there is a need for thrusters beyond these conventional technologies. In particular, we need systems that more easily scalable to higher power (> 1 MW) can be used with a multitude of propellants (as opposed to the inert gases typically used on Hall and ion thrusters), and capable of dual mode operation [3, 4]

One such alternative is the field-reversed configuration thruster (FRC). The FRC is a form of pulsed propulsion that utilizes the repeated formation and ejection of magnetically isolated plasma bodies called plasmoids. As the thrusters are inductively coupled, they can be used with a variety of propellants [5]. Therefore, FRCs open up a wide mission parameter space and can potentially be integrated with a spacecraft system and mission architecture incorporating in situ-resource utilization technology [6].

Multiple techniques exist for generating the azimuthal current including, but not limited to, using planar coils and the conical -pinch technique [7]. The focus of this study is FRCs utilizing rotating magnetic fields for azimuthal current generation, or RMF-FRCs. RMFs are a particularly attractive option for driving currents as the fields can penetrate into the plasma much farther than the classical skin depth resulting in more efficient power deposition as the fields couple to with increasing RMF amplitude. RMF-FRCs originated in the fusion community where the rotating magnetic field current drive is used for plasma confinement [8, 9]. Subsequently, it was found that by inducing a radial gradient in the steady background field, the plasmoid could be ejected at high velocities for use as a pulsed propulsion device. Initially, two plasmoids were produced and accelerated towards each other to achieve fusion [10]. The concept has generated interest in the electric propulsion community. The Air Force Research Laboratory (AFRL) has contributed substantially to simulating and testing the devices [11]. The private company, MSNW LLC has developed prototypes of the thruster and have tested the units. In addition, they have derived simple scaling expressions to gain insight into the performance of the thrusters [5].

To date, no thrust has not been measured for RMF-FRC's. There are fundamental questions related to the overall performance of these devices. In particular, there are still several open questions pertaining to efficiency and specific impulse scaling with input energy. It is apparent that new scaling laws are needed to increase fundamental insight, better predict performance, and ultimately guide thruster design. As a first order approach to this problem, we have constructed a simple lumped circuit model of the system. To this end, we construct a lumped circuit model of the system. Reducing key components of inductive thrusters to a simple circuit has long been used to model pulsed propulsion devices including pulsed inductive thrusters and annular FRC's [12–14]. The goal is to see if we can determine physical trends and dependencies that may inform the design and testing of these devices. With this end in mind, this paper is organized in the following way. We first provide a brief review of fundamental RMF-FRC operation. Then, we create an equivalent circuit that consists of key elements of the propulsion system. Next, we will solve the governing system of electrical and relevant physical equations to, ideally, produce a set of scaling laws that relate circuit elements, geometry, and power to efficiency and specific impulse. We numerically solve the system of equations and plot the results to identify any notable trends. We examine these governing equations in asymptotic limits to generate analytical expressions to gain further insight into the numerically observed trends. We conclude by identifying further techniques to enhance the model to provide a more coherent and insightful physical model.

III. Overview of RMF-FRC Operation

WE consider in here an idealized case fo RMF-FRC operation to illustrate their fundamental of operation. This follows the treatment of Slough et al reference [5]. RMF-FRCs operate by inducing azimuthal currents in a plasma column confined by a steady background axial magnetic field. At a threshold value, the magnetic field resulting from the flowing azimuthal current reverses the background axial field near the plasma centerline, resulting in a self-contained

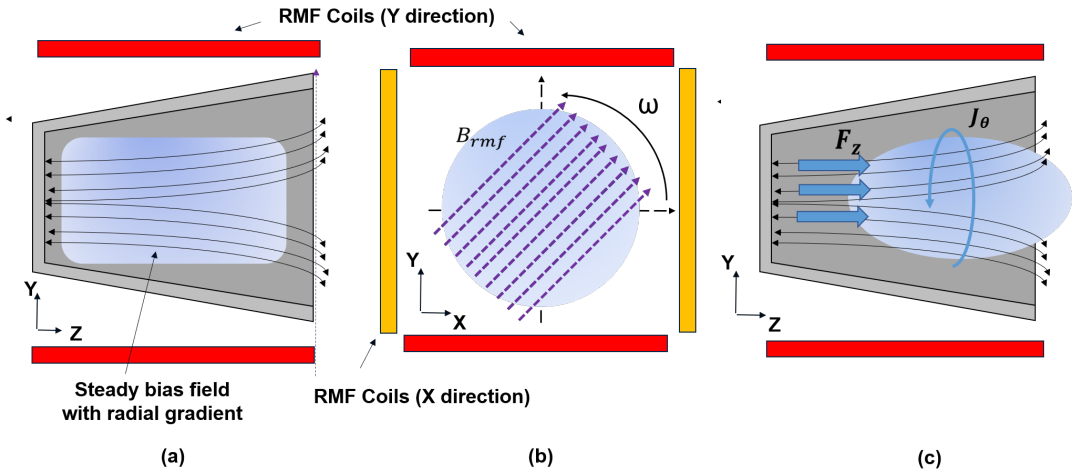

Fig. 1 RMF-FRC Operation - (a) Ionized gas is injected into the thruster cone. A steady bias magnetic field with radial gradient is present. (b) Two sets of coils oriented in the x and y directions are used to generate a rotating magnetic field (RMF) by driving sinusoidal currents 90° out of phase at frequency w. The RMF induces axial and azimuthal currents. (c) The FRC is formed. Large azimuthal currents in the plasma interact with the external radial magnetic field which drives the plasmoid out of the thruster via the Lorentz Force.

magnetic structure populated by a high density plasma. This magnetic plasmoid is then accelerated by a Lorentz force that results when the azimuthal currents in the plasmoid interact with a gradual radial gradient in the background field. Fig. 1 illustrates the process. Ionized gas fills the thruster chamber with a background steady magnetic field of the form

$$\vec{B}_s = B_{s,r}\hat{r} + B_{s,z}\hat{z}, \tag{1}$$

where $B_{s,r}$ and $B_{s,z}$ are the radial and axial components of the bias field respectively. Two sets of coils arranged perpendicular to each other alternating magnetic fields 90°out of phase. The combined effects of each coil creates a rotating magnetic field of the form

$$\vec{B}_{RMF} = B_o \cos(\omega t - \theta)\hat{r} + B_o \sin(\omega t - \theta)\hat{\theta} = B_{r,ext}\hat{r} + B_{\theta,ext}\hat{\theta}, \tag{2}$$

where B_o is the amplitude of the magnetic field and ω is the frequency at which the field rotates. This is an idealized RMF. The fields have no radial or axial dependence. In our model, we assume the RMF is the idealized form presented by equation 2. This is to illustrate qualitatively the performance of the devices in order to find a simplified form for the B-field. We note that this form of the field is relaxed in a more self-consistent analysis. We assume that they are not affected by the loading of the plasma during discharge and maintain a sinusoidal θ dependence. The only effects of plasma loading on the RMF is due to the change in magnitude of their currents. Using Faraday's law of induction and the generalized Ohm's law for an infinitely long plasma column with negligible axial and azimuthal pressure gradients, the time varying magnetic field produces an electric field that drives an axial and azimuthal current,

$$J_z(t,r,\theta) = \frac{\omega r B_{r,ext}}{\eta} - \frac{ne\omega r(B_{r,ext} + B_{s,r}\hat{r})}{\eta ne\left(1 + 2\left(\frac{\eta ne}{B_o}\right)^2\right)}, \tag{3}$$

$$J_\theta(t,r) = -\frac{ne\omega r}{1 + 2\left(\frac{\eta ne}{B_o}\right)^2}, \tag{4}$$

where n is the electron density (assumed to be constant in this study) e is the elementary charge, and η is the resistivity defined as

$$\eta = \frac{m\nu_{ei}}{ne^2}. \tag{5}$$

Here, ν_{ei} is the electron-ion collision frequency and m is the mass of an electron. The azimuthal current interacts with the radial component of the steady bias field to produce an axial Lorentz force that drives the plasmoid out of the thruster at high speeds:

$$F_z = \int_V J_\theta B_{s,r} dV \tag{6}$$

The key insight from this result is that the acceleration mechanism for these devices is largely driven by the current induced in the azimuthal direction coupling with the applied magnetic field. This suggests that by finding simple models for these parameters, we can evaluate performance. This is what we attempt to do with a lumped circuit model in the next section.

IV. Performance Model

A. Review of Lumped Circuit Modeling

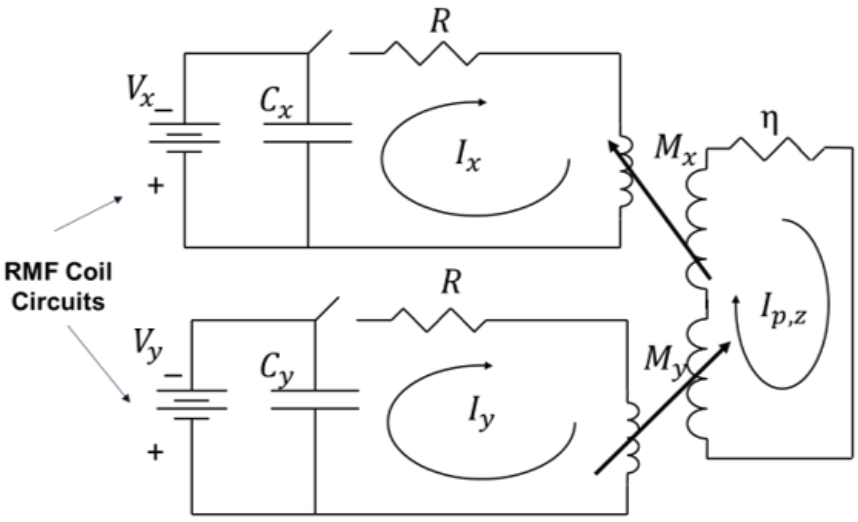

Fig. 2 Lumped circuit of an RMF-FRC

EP systems are inherently electrically complicated which can make a comprehensive analysis of the device difficult. To circumvent this issue, the system can be reduced to just a few simple key elements coupled together that greatly simplify the circuit while retaining the relevant physics of thruster operation. To date, several lumped circuit models have been developed for various inductive plasma thrusters. FRC's are no exception. Typical models simplify the driving circuit as a charged capacitor in series with resistance, and inductor representing the induction coil coupled to a conducting slug representing the plasma body with its own self inductance and plasma. Transformer nomenclature is typically used when describing such systems. A critical parameter describing the behavior of the thrusters using this technique is calculating the mutual inductance and accurately modeling how it changes as the slug is accelerated out of the thruster. Mutual inductance has been studied and modeled extensively for electromagnetic inductors [15]. J. Bernades and S. Merryman provided an empirical expression for mutual inductance as a function of position for ring shaped conductors accelerated by a driving coil. The expression was derived by directly measuring the mutual inductance at various positions and fitting a curve to the data points [16]. While calculated for ring shaped inductors, the mutual inductance model coupled with a lumped circuit was shown to reasonably predict performance of pulsed plasmoid thrusters utilizing various geometries [17]. Furthermore, Hill used the mutual inductance expression to predict performance of annular FRC's (AFRC) [13, 18]. Nevertheless, there are several shortcomings and questions regarding antennae-plasmoid coupling for RMF-FRC's that we wish to investigate. As opposed to the model presented by J. Bernades and S. Merryman, we wish to directly model the mutual inductance by calculating flux expressions caused by

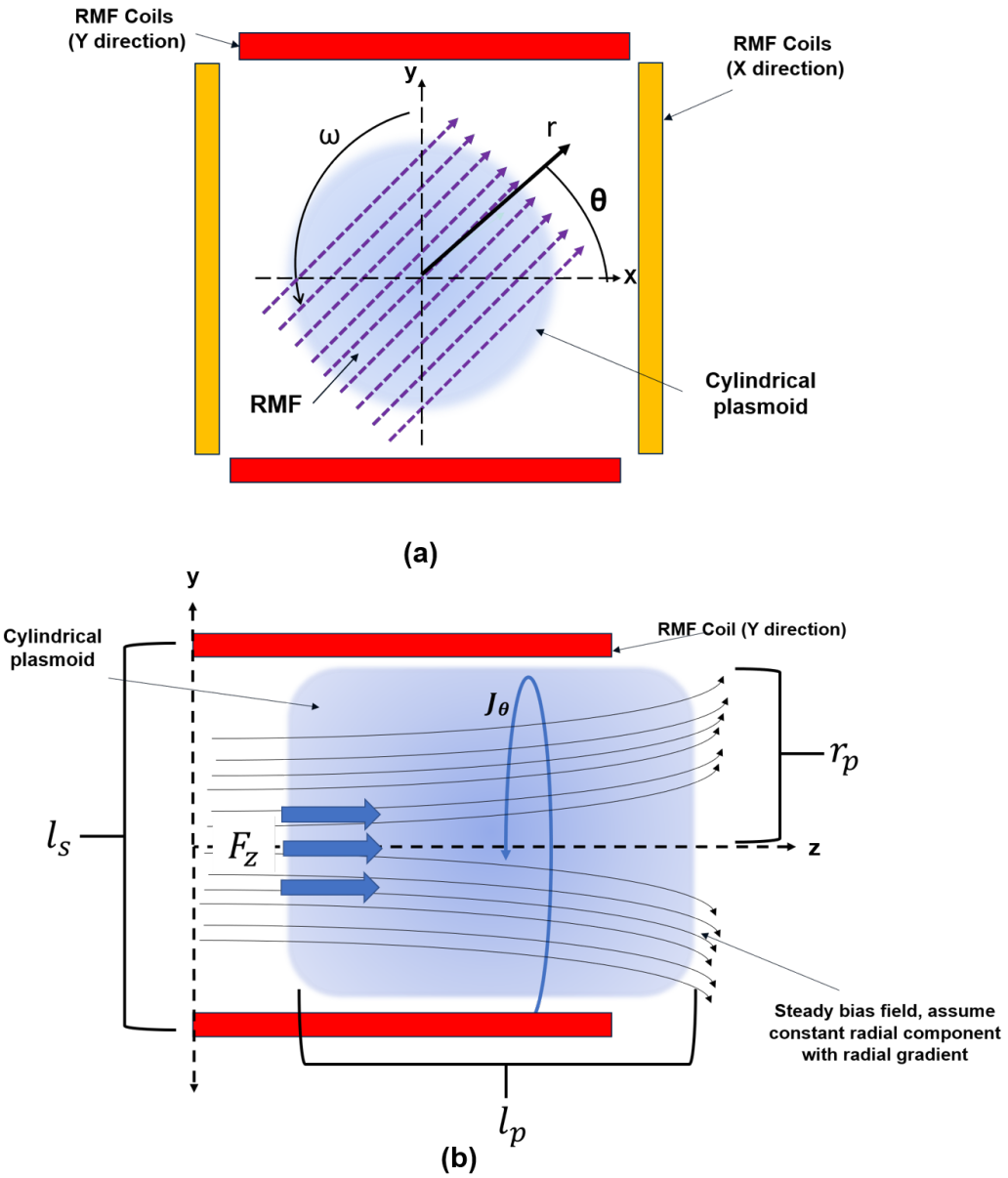

Fig. 3 Simplified thruster geometry used in performance model. (a) front view (b) side view

the plasmoid onto the RMF antennae resulting in back emf and ultimately affecting the coil and plasma currents. Such methods were successfully used to model the plasma currents and RMF penetration into the plasmoid by W. N. Hugrass et al [19]. However, the circuit model used by the authors was for fusion purposes and did not include the effects of the plasmoid translating through the inductive region. We attempt to model such effects in this study. J. Little et al used a lumped circuit to model a potential second stage for an RMF-FRC consisting of a series of flux coils downstream of the RMF coils. The flux coils are pulsed as the plasmoid traverses downstream, adding energy to the plasma body [20]. Expressions for the mutual inductance were derived using plasma current equilibrium expressions derived by Solov'ev [21]. Thus, expressions for the flux produced by the plasmoid during its acceleration in the RMF region are still unknown. We derive a performance model with the lumped circuit approximation and incorporate affects of the flux produced by the plasmoid as it accelerates out of the thruster.

B. RMF-FRC Circuit Model

In its simplest form, an RMF-FRC can be modeled as two driving circuits, each representing a pair of RMF coils, coupled to a cylindrical, conducting slug representing the plasmoid. Fig. 2 provides a schematic of the lumped circuit. In each driving circuit, a capacitor is charged to an initial voltage, V_o. At $t = 0$, the capacitor for the set of coils in the x-direction begins to discharge. A quarter period later, the capacitor for the y-direction set of coils discharges. Like all RLC circuits, the system will ring down, producing current oscillations. Due to each circuit using identical components, the delay between discharges will result in the currents being 90° out of phase with each other. The resulting magnetic field produced by the coils will interact and propel the conducting slug in a manner similar to that described in section II. Fig. 3 illustrates the simplified geometry used for our model with with relevant geometric values labeled.

C. System Equations

Using Fig. 2 as a template, we begin to construct our circuit equations using Kirchhoff's Voltage Law for each RMF coil:

$$V_x(t) + RI_x(t) + LI_x'(t) = k\Phi_x'(t) \tag{7}$$

$$V_y(t) + RI_y(t) + LI_y'(t) = k\Phi_y'(t) \tag{8}$$

where k is the coupling factor between the RMF coils and the plasmoid. It represents takes into account non-idealities in coupling such as non-uniform fields and is left as a free parameter in our analysis. $V_x(t)$ and $V_y(t)$ are defined, respectively, by:

$$V_x'(t) = \frac{I_x(t)}{C} \tag{9}$$

$$V_y'(t) = \frac{I_y(t)}{C} \tag{10}$$

$\Phi_x'(t)$ and $\Phi_y'(t)$ are the time derivatives of the flux produced by the plasmoid on the x- and y-direction RMF coils respectively. To simplify the model, we assume the ideal case of an infinitely long plasma column. We can define our RMF in terms of the coil currents:

$$\vec{B}_{RMF} = \frac{\mu_o N}{l_s}(I_x(t)\cos(\theta)\hat{x} + I_y(t)\sin(\theta)haty). \tag{11}$$

When acted upon by the field represented by equation 11, the slug will produce a rotating magnetic field of its own. It is this field that will couple with the RMF coils. To see this, we can calculate the magnetic flux produced by the slug. Using equation 7 in conjunction with Faraday's law of induction and the generalized Ohm's law once again, we can re-derive the axial current density in terms of the RMF coil currents, I_x and I_y:

$$J_z = -\frac{r\frac{\mu_o N}{l_s}(-I_x'(t)\sin(\theta) + I_y'(t)\cos(\theta))}{\eta} + \frac{r\left(\frac{\mu_o N}{l_s}\right)^2\left((B_{s,r} + \frac{\mu_o N}{l_s}(I_x(t)\cos(\theta) + I_y(t)\sin(\theta))(-Iy(t)Ix'(t) + Ix(t)Iy'(t)\right)}{\eta^3 n^2 e^2\left(2 + \frac{2B_{s,r} + \left(\frac{\mu_o N}{l_s}\right)^2(Ix(t)^2 + Iy(t)^2)}{\eta^2 n^2 e^2}\right)} \tag{12}$$

Using the Biot-Savart law, we can calculate the magnetic flux produced by the axial plasma current that intersects the RMF coils. To further simplify the problem, we assume that the magnetic field produced at centerline in each direction is constant over the entire flux area for the RMF coils. The area is simply the cross-sectional area of the plasmoid which changes over time as the plasmoid accelerates out of the induction zone. We denote it as:

$$A(t) = 2r_p(l_p - z(t)). \tag{13}$$

r_p and l_p are the radius and length of the plasmoid while *z(t)* is the position of the plasmoid's trailing end. l_p is also the length of the induction zone reflecting the scenario in which ionized gas initially fills the entire chamber. Thus, as

z(t) approaches l_p, the mutual inductance goes to zero. Consequently, this model is not valid beyond *z(t)* = l_p, as the coupling would reverse.

Using our formulation for *A(t)*, the resulting flux equations in the x- and y- directions for the x-and y-oriented RMF coils respectively are:

$$\Phi_x(t) = -\frac{A(t)(2l_p^2 r_p^2 + r_p^4)\frac{\mu_o N}{l_s}\left(\left(2(B_{s,r}^2 + e^2n^2\eta^2) + \left(\frac{\mu_o N}{l_s}\right)^2 I_x(t)^2\right)I_x'(t) + \left(\frac{\mu_o N}{l_s}\right)^2 I_x(t)I_y(t)I_y'(t)\right)}{16l_p^2\eta\left(2(B_{s,r}^2 + e^2n^2\eta^2) + \left(\frac{\mu_o N}{l_s}\right)^2 (I_x(t)^2 + I_y(t)^2)\right)} \tag{14}$$

$$\Phi_y(t) = -\frac{A(t)(2l_p^2 r_p^2 + r_p^4)\frac{\mu_o N}{l_s}\left(\left(2(B_{s,r}^2 + e^2n^2\eta^2) + \left(\frac{\mu_o N}{l_s}\right)^2 I_y(t)^2\right)I_y'(t) + \left(\frac{\mu_o N}{l_s}\right)^2 I_y(t)I_x(t)I_x'(t)\right)}{16l_p^2\eta\left(2(B_{s,r}^2 + e^2n^2\eta^2) + \left(\frac{\mu_o N}{l_s}\right)^2 (I_x(t)^2 + I_y(t)^2)\right)} \tag{15}$$

The capacitor for the y-direction RMF coil is discharged 90° out of phase with the x-direction RMF coil. The azimuthal current can be expressed in terms of the RMF coil currents as *z(t)* can be calculated using the acceleration of the plasmoid as defined by equation 6. First, we put the azimuthal current in terms of circuit parameters:

$$J_\theta(t, r, \theta) = \frac{r\left(\frac{\mu_o N}{l_s}\right)^2 (I_x'(t)I_x(t) + I_y'(t)I_y(t))}{en\eta^2\left(2 + \frac{2B_{s,r}^2 + \left(\frac{\mu_o N}{l_s}\right)^2 (I_x(t)^2 + I_y(t)^2)}{e^2n^2\eta^2}\right)} \tag{16}$$

Using equation 6 and integrating over the plasmoid volume undergoing acceleration in the induction zone, the acceleration of the plasmoid can be computed, thus providing the axial position of the slug at a time *t*:

$$z''(t) = \frac{2B_{s,r}en\pi r_p^3\left(\frac{\mu_o N}{l_s}\right)^2 (l_p - z(t))(I_y(t)I_x'(t) - I_x(t)I_y'(t))}{3M\left(2(B_{s,r}^2 + e^2n^2\eta^2) + \left(\frac{\mu_o N}{l_s}\right)^2 (I_x(t)^2 + I_y(t)^2)\right)} \tag{17}$$

where *M* is the mass of the plasma slug.

Finally, the efficiency is calculated using the kinetic energy of the plasma slug when exiting the thruster and the total energy initially stored in the capacitors:

$$\eta_E = \frac{KE}{E_o} = \frac{\frac{1}{2}Mu_{ex}^2}{CV_o^2} \tag{18}$$

where u_{ex} is the exit velocity of the plasma slug and V_o is the initial voltage of the capacitors.

V. Results

Equations 7 - 18 form our full system of equations. Solving them over a range of initial voltages allows us to calculate the specific impulse and efficiency as a function of input energy as well as coupling factors. We discuss two cases to help gain more physical insight into RMF-FRC operation.

A. Fixed RMF Frequency Case

If we first consider the case in which the frequency of the ring down of the RMF circuits is fixed, analytical solutions for the impulse and efficiency can be derived by solving the relevant equations. Physically, this case represents the electrons moving synchronously with the RMF. The azimuthal current is fixed and the axial plasma current density is screened out. Since the axial current density approaches zero, the back emf caused by the plasma currents onto the RMF coils goes to zero as well, simplifying equations 7 and 8 (k is set to zero). Solving equations 7 - 9 yields the familiar current waveforms for an LRC circuit. The current equation for the y-direction RMF coils have been adjusted to represent the 90° phase difference:

$$I_x(t) = \frac{-V_o e^{-\alpha t}}{L\omega} \sin(\omega t) \tag{19}$$

$$I_y(t) = \frac{-V_o e^{-\alpha t}}{L\omega} \cos(\omega t) \tag{20}$$

where ω and α are the frequency and damping factor respectively for the discharging circuit and are defined as

$$\omega = \sqrt{\frac{1}{LC} - \frac{R^2}{4L^2}} \tag{21}$$

and

$$\alpha = \frac{R}{2L}. \tag{22}$$

We substitute equations 19 and 20 into equation 16 and simplify to obtain the azimuthal current density profile:

$$J_\theta(t, r) = \frac{ne\omega r}{1 + 2\left(\frac{ne\eta l_s L^2 \omega^2}{-\mu_o^2 N^2 V_o^2 e^{-2\alpha t}}\right)} \tag{23}$$

The force is calculated using equation 6 and integrating over the thruster chamber volume:

$$F_z(t) = \int_0^{l_p}\int_0^{2\pi}\int_0^{r_p} \frac{ne\omega r^2 B_{s,r}}{1 + 2\left(\frac{ne\eta l_s L^2 \omega^2}{-\mu_o^2 N^2 V_o^2 e^{-2\alpha t}}\right)} dr d\theta dz = \frac{2\pi ne\omega l_p r_p^3 B_{s,r}}{3 + 6\left(\frac{ne\eta l_s L^2 \omega^2}{-\mu_o^2 N^2 V_o^2 e^{-2\alpha t}}\right)} \tag{24}$$

Next, we calculate the total impulse by integrating the force over the full discharge time:

$$I = \int_0^\infty F_z dt = \frac{2\pi en\omega r_p^3 l_p B_{s,r}}{3\alpha} ln\left(1 + \frac{E_o \mu_o^2 N^2}{2CL^2 l_s^2 \omega^2 (B_{s,r}^2 + e^2 n^2 \eta^2)}\right). \tag{25}$$

The expression for impulse can be rewritten in terms of the maximum force possible, $F_{z,max}$:

$$I = \frac{F_{z,max}}{\alpha} ln\left(1 + \frac{E_o \mu_o^2 N^2}{2CL^2 l_s^2 \omega^2 (B_{s,r}^2 + e^2 n^2 \eta^2)}\right) \tag{26}$$

where the max force is defined as:

$$F_{z,max} = \frac{2}{3}\pi en\omega r_p^3 l_p B_{s,r}. \tag{27}$$

$F_{z,max}$ corresponds to the force produced at constant frequency and background magnetic field when the electrons are fully tied to and rotate with the RMF. In this scenario, the maximum azimuthal current density is:

$$J_{\theta,max} = en\omega r \tag{28}$$

The total impulse scales logarithmically with E_o and linearly with $F_{z,max}$. It also scales inversely with the damping factor, which is the inverse of the characteristic time of the discharging RMF coils. Thus, higher impulse is obtained during shorter discharge times.

The efficiency can be calculated from the impulse:

$$\eta_E = \frac{KE}{E_o} = \frac{I^2}{2ME_o} = \frac{\left[\frac{F_{z,max}}{\alpha} ln\left(1 + \frac{E_o \mu_o^2 N^2}{2CL^2 l_s^2 \omega^2 (B_{s,r}^2 + e^2 n^2 \eta^2)}\right)\right]^2}{ME_o}. \tag{29}$$

Here we see that the efficiency scales both logarithmically and inversely with the input energy. The implications of this expression will be discussed in detail in Section VI.

B. Coupled Cases

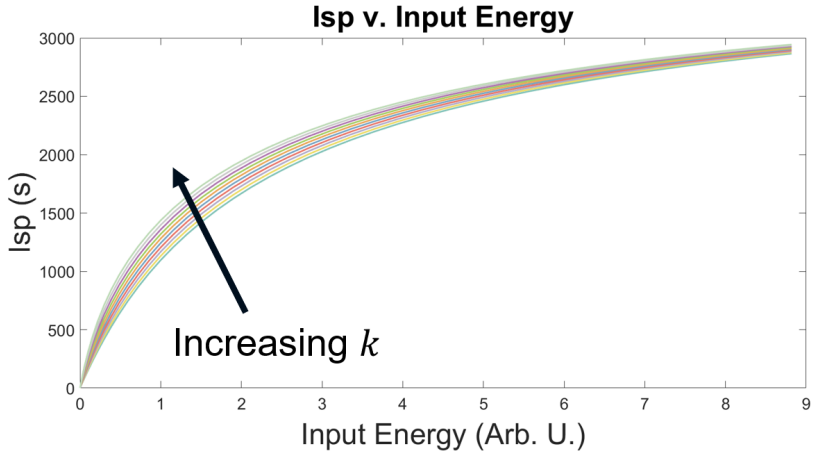

Fig. 4 Specific impulse as a function of input energy normalized to input energy at maximum efficiency

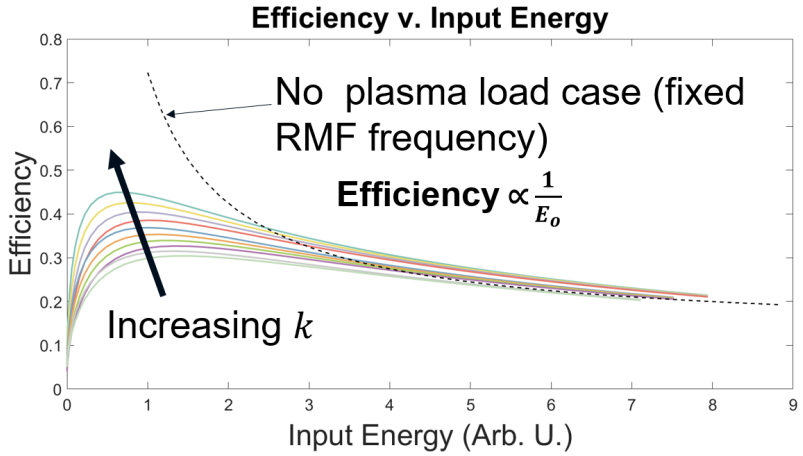

Fig. 5 Efficiency impulse as a function of input energy normalized to input energy at maximum efficiency

Cases in which the frequency is not fixed must be solved numerically. Mathematica is used to solve the full system of equations for various values of . Figs. 4 and 5 plot the specific impulse and efficiency respectively as a function of the input energy. The input energy is normalized by the input energy corresponding to the maximum efficiency. The propellant is Xenon gas. The following parameter values were chosen for this study: $n = 10^{18}\ m^{-3}$, $\eta = 5.89^{-6}\ \Omega$ -m, $B_{s,r} = 0.1$ T, $l_s = 0.2$ m, $r_p = 0.1$ m, $N = 2$, $l_p = 0.4$ m, $R = 0.3\ \Omega$, and $C = 0.04$ nF. The initial voltage, V_o, was varied from 0 to 20,000 V while the coupling fact, k, was varied from 0 to 1000 in increments of 100.

VI. Discussion

We discuss here some of the trends identified in Section V. Both the magnitude of the maximum efficiency and specific impulse for a given input energy increases with increased feedback from plasma to the RMF coils. This feedback re-circularizes power back into the circuit (i.e. the plasma is better coupled to the driving circuit). The I_{sp} increases rapidly for low energies. At higher energies it begins to plateau. I_{sp}, as plotted in Fig. 4, increases rapidly for low input energies. At higher energies the increase is more gradual.

The efficiency as a function of input energy is plotted in Fig. 5. Like the I_{sp}, efficiency increases rapidly at lower input energies. There is a peak before it drops off sharply with increasing energy. A similar trend for pulsed plasmoid thrusters was projected by A. Martin and R. Eskridge [17]. However, little explanation is given for what causes the trend. Our analysis provides a plausible reason for why we may see the observed efficiency trend in an RMF-FRC. As the RMF magnitude increases, electrons become increasingly magnetized (overcome collisions) and are subsequently tied to and rotate synchronously with the RMF field lines. For a sufficiently large magnetic field, the electrons become fully magnetized (collision-less) and a maximum azimuthal current is achieved. This effect can be observed by taking the limit of equation 4 in the regime of high magnetic field amplitudes, the fluid equation solution for the azimuthal current density. At high magnetic field magnitudes, the azimuthal current reaches its maximum amplitude and is given by equation 28. Thus, increasing RMF coil currents beyond this point results in no significant increase in the overall force (this also results in an effective cap for exhaust velocity), additional energy is wasted, and the efficiency gradually decreases for higher input energies. As the electrons are rotating synchronously with the magnetic field, we can use equation 29 in the limit of high input energy to derive a scaling expression for the efficiency (trend line is also shown in Fig. 5):

$$\eta_{E,E_o\to\infty} \propto \frac{1}{E_o}. \tag{30}$$

The mechanism behind the azimuthal current density cap is a feature unique to RMF-FRC operation. It indicates that there is an optimal operating condition for an RMF-FRC of given geometry and circuit elements. However, it is possible that the decreasing efficiency trend that we observe in our RMF-FRC model is the result of the plasmoid being accelerated, and thus decoupled, from the thruster before energy from the capacitors can be deposited into it. Higher specific impulse would result in lower efficiencies as the plasmoid decouples faster. Indeed, this may have been the mechanism in Martin and Eskridge as their coupling to the plasma in the current was independent of the RMF mechanism. A more comprehensive circuit parameter analysis is required to fully assess what causes the efficiency to decrease rapidly. Hill performed such an analysis on AFRC's to provide more insight into thruster design [18]. The EP community could benefit greatly from a similar study for RMF-FRC's. Nevertheless, our model can be improved significantly by readdressing some of the simplifying assumptions made for our model. The plasma self-inductance was not considered, the radial component of the steady bias field was assumed to be constant in space (as opposed to having an axial gradient), and an infinitely long plasma geometry was used. While it simplified the problem, it is an idealized model.

VII. Conclusion

We presented a review of RMF-FRC operations and constructed a circuit model representing thruster operation. We derived performance model equations and utilized assumption to simplify the system were discussed. We examined analytical and numerical results in the context of specific impulse and efficiency observations. The results show that performance increases with increasing coupling factor. The I_{sp} increases rapidly at low input energies before gradually plateauing at higher energies. The efficiency also increases rapidly with low input energies. However, it peaks before decaying, following the scaling of $1/E_o$. The plasma self-inductance, radial steady magnetic field, and infinitely long cylindrical plasma assumptions will be addressed in future models to increase insight of fundamental thruster operation.

References

[1] Jahn, R. G., *Physics of Electric Propulsion*, McGraw-Hill Inc., New York, 1968, Chaps. 1,9.

[2] Hall, S. J., *Chracterization of a 100-kW Class Nested-Channel Hall Thruster*, University of Michigan, PhD Dissertation, 2017.

[3] "Air Force Research Laboratory high power electric propulsion technology development," *IEEE Aerospace Conference*, Big Sky, Montana, 2010.

[4] "NASA Technology Roadmaps TA 2: In-Space Propulsion Technologies," NASA, Washington, DC, July 2015.

[5] Slough, K. D., J, and Weber, T., "Spacecraft Thermal Control, Design, and Operation," *31st International Electric Propulsion Conference*, Ann Arbor, Michigan, 2009.

[6] Simon, T., and K, S., "NASA In-Situ Resource Utilization (ISRU) Development and Incorporation Plans," *Technology Exchange Conference*, Galveston, Texas, November 2007.

[7] Greve, H. J. K. J., P, and Ulrich, L. K., "Effects of an inhomogeneous impurity distribution in a field-reversed theta-pinch," *Physics of Fluids*, Vol. 25, No. 3, 1982, pp. 452–456.

[8] Blevin, A., H, and Thonemann, P. C., "Plasma Confinement Using an Alternating Magnetic Field," *Nuclear Fusion Supplement Part I*, 1962, p. 55.

[9] Brunkhorst, B. B. F. N., C, and Cohen, S. A., "The Princeton FRC Rotating-Magnetic-Field Experiment RF System," *IEEE 22nd Symposium on Fusion Engineering*, Champaign, Illinois, 2007.

[10] Turchi, P. J., "An Electric Propulsion System Based on Controlled Fusion and Electromechanical Energy Conversion," *33rd International Electric Propulsion Conference*, Washington, D. C., October 2013.

[11] Justin, M. R., K, and Sousa, E. M., *High Fidelity Modeling of Field-Reversed Configuration (FRC) Thrusters*, Air Force Research Laboratory, AFRL-RQ-ED-TR-2017-0002, Edwards Air Force Base, California, April 2017.

[12] Mikellides, P. G., *Pulsed Inductive Thruster (PIT): Modeling and Validation Using the MACH2 Code*, NASA, CR–2003-212714, Dec. 2003.

[13] Hill, C., *Translation Studies on an Annular Field Reversed Configuration Device for Space Propulsion*, Michigan Technological University, PhD Dissertation, 2012.

[14] Mikellides, P. G., *The PIT MkV Pulsed Inductive Thruster*, NASA Contractor Report 191155, 1993.

[15] Novac, S. I. R. E. M. C., B M, and P, S., "Studies of a Very High Efficiency Electromagnetic Launcher," *Journal of Physics D-Applied Physics*, , No. 35, 2002, pp. 1447–57.

[16] Bernardes, J., and Merrymann, S., "Parameter Analysis of a Single Stage Induction Mass Driver," *5th IEEE International Pulsed Power Conference*, Albuquerque, New Mexico, 1983.

[17] Martin, A., and Eskridge, R., "Electrical Coupling Efficiency of Inductive Plasma Accelerators," *Journal of Physics D-Applied Physics*, Vol. 38, No. 23, 2005, pp. 4168–4179.

[18] "Numerical Optimization of an Annular Field Reversed Configuration Translation Experiment," *31st International Electric Propulsion Conference*, Ann Arbor, Michigan, September 2009.

[19] Hugrass, O. T., W N, and Ohnishi, M., "Plasma-circuit Interactions in Rotating Magnetic Field Current Drive," *Plasma Physics and Controlled Fusion*, Vol. 50, February 2008, p. 055008.

[20] "Scaling of FRC Thrusters with Neutral Entrainment," *8th JANNAF Spacecraft Propulsion Subcommittee Meeting*, Phoenix, Arizona, December 2016.

[21] Ji, Y. M. K. R. P. N., H, and Himura, H., "Studies of Global Stability of Field-Reversed Configuration Plasmas Using a Rigid Body Model," *Physics of Plasmas*, Vol. 5, No. 10, 1998, pp. 3685–3693.